

# Mutation in a short-chain collagen gene, *CTRP5*, results in extracellular deposit formation in late-onset retinal degeneration: a genetic model for age-related macular degeneration

Caroline Hayward<sup>1,†</sup>, Xinhua Shu<sup>1,†</sup>, Artur V. Cideciyan<sup>2</sup>, Alan Lennon<sup>1</sup>, Perdita Barran<sup>3</sup>, Sepideh Zarepari<sup>4</sup>, Lindsay Sawyer<sup>5</sup>, Grace Hendry<sup>1</sup>, Baljean Dhillon<sup>6</sup>, Ann H. Milam<sup>2</sup>, Philip J. Luthert<sup>7</sup>, Anand Swaroop<sup>4</sup>, Nicholas D. Hastie<sup>1</sup>, Samuel G. Jacobson<sup>2</sup> and Alan F. Wright<sup>1,\*</sup>

<sup>1</sup>MRC Human Genetics Unit, Western General Hospital, Crewe Road, Edinburgh, UK, <sup>2</sup>Department of Ophthalmology, Scheie Eye Institute, University of Pennsylvania School of Medicine, Philadelphia, PA, USA, <sup>3</sup>School of Chemistry, University of Edinburgh, Edinburgh, UK, <sup>4</sup>Departments of Ophthalmology and Visual Sciences, and Human Genetics, University of Michigan, Ann Arbor, MI, USA, <sup>5</sup>Institute of Cell and Molecular Biology, University of Edinburgh, Edinburgh, UK, <sup>6</sup>Department of Ophthalmology, Royal Infirmary of Edinburgh, University of Edinburgh, Edinburgh, UK and <sup>7</sup>Department of Pathology, Institute of Ophthalmology, University College London, London, UK

Received June 17, 2003; Revised August 7, 2003; Accepted August 15, 2003

**A primary feature of age-related macular degeneration (AMD) is the presence of extracellular deposits between the retinal pigment epithelium (RPE) and underlying Bruch's membrane, leading to RPE dysfunction, photoreceptor death and severe visual loss. AMD accounts for about 50% of blind registrations in Western countries and is a common, genetically complex disorder. Very little is known regarding its molecular basis. Late-onset retinal degeneration (L-ORD) is an autosomal dominant disorder with striking clinical and pathological similarity to AMD. Here we show that L-ORD is genetically heterogeneous and that a proposed founder mutation in the *CTRP5* (*C1QTNF5*) gene, which encodes a novel short-chain collagen, changes a highly conserved serine to arginine (Ser163Arg) in 7/14 L-ORD families and 0/1000 control individuals. The mutation occurs in the gC1q domain of *CTRP5* and results in abnormal high molecular weight aggregate formation which may alter its higher-order structure and interactions. These results indicate a novel disease mechanism involving abnormal adhesion between RPE and Bruch's membrane.**

## INTRODUCTION

Late-onset retinal degeneration (L-ORD) is an autosomal dominant disorder characterized by onset in the fifth to sixth decade with night blindness and punctate yellow-white deposits in the retinal fundus, progressing to severe central and peripheral degeneration, with choroidal neovascularization and chorioretinal atrophy (1–5). The prevalence of L-ORD is unknown, but it is thought to be uncommon. The disease is associated with a thick extracellular sub-RPE deposit between

the basal lamina of the retinal pigment epithelium (RPE) and Bruch's membrane, extending from the central retina to the ora serrata (Fig. 1A and B). It contains protein and lipid and consists of an inner collagenous/mucopolysaccharide layer, an outer lipid layer and a layer of neovascularization between the elastin layer of Bruch's membrane and the RPE (1,2). In later stages, there is widespread loss of RPE and photoreceptors, with choroidal neovascularization and disciform macular scarring (1,2,4,5). The presence of both focal and diffuse sub-RPE deposits is also a feature in age-related macular

\*To whom correspondence should be addressed. Tel: +44 1314678437; Fax: +44 1314678456; Email: alan.wright@hgu.mrc.ac.uk

<sup>†</sup>The authors wish it to be known that, in their opinion, the first two authors should be regarded as joint First Authors.

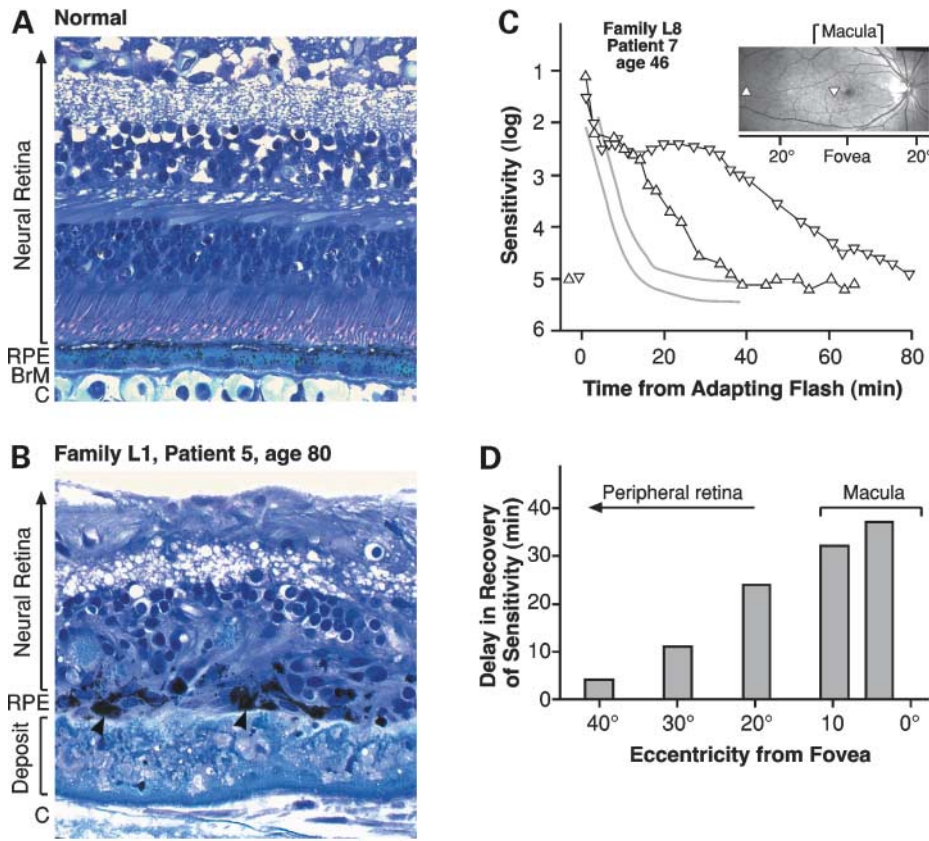


**Figure 1.** Phenotype of L-ORD by histopathology and visual testing. (A) Normal human retina has a thin Bruch's membrane (BrM) between the retinal pigment epithelium (RPE) and choroid (C). The RPE is uniform in thickness with melanin granules in the apical portions of the cells. The neural retina has a normal number and distribution of cells for this locus (edge of macula). (B) L-ORD retina has a thick layer of extracellular deposits (bracket) between RPE and choroid. The RPE cells are reduced in number and size, and are heavily pigmented (arrowheads). The neural retina is degenerate with loss of cells and abnormal architecture. Bar = 100  $\mu$ m. (C) Psychophysically measured dark adaptation in L-ORD demonstrating large delay in recovery of rod sensitivity following a flash estimated to isomerize 14% of rhodopsin. Two functions represent data obtained at 4 and 30° eccentric in the temporal retina (insert); normal (mean  $\pm$  2SD) results delimited by gray lines. (D) The delay in recovery of sensitivity shows dramatic regional retinal variation with the greatest abnormality in the macula and less abnormality in peripheral retina.

degeneration (AMD), which is a genetically complex disorder affecting up to 30% of the elderly population and which accounts for 50–60% of new blind registrations in Western countries (6,7). The sub-RPE deposits in L-ORD have been investigated and are similar histopathologically to those found in the macula in AMD (1,2). However, over 100 different proteins have been found in AMD deposits (8) so that it is difficult to dissect primary from secondary disease mechanisms. L-ORD is distinct from AMD in its Mendelian inheritance and the more extensive distribution of sub-RPE deposits and atrophy, leading to loss of both central and peripheral vision. It differs from another autosomal dominant condition, Sorsby fundus dystrophy (SFD), in its slightly later onset of night blindness and less prominently haemorrhagic macular degeneration (9). SFD results from mutations in the *TIMP3* gene and maps to chromosome 22. The chromosomal localization of L-ORD has not been reported. Here we describe the genetic mapping of an extended L-ORD kindred to chromosomal region 11q23 and the identification of a proposed causal gene.

## RESULTS

To map the L-ORD locus genetically, we sought a phenotypic marker to increase the number of inferred gene carriers among asymptomatic family members. Delays in the kinetics of dark adaptation, implying RPE dysfunction, were detectable decades before the eye disease became overt (1–3). The distribution of dark adaptation abnormalities across the retina in L-ORD was found to be more pronounced in the macula than in peripheral retina (Fig. 1C and D), as also found in AMD (10,11).

A 10 cM genome scan was carried out in an extended L-ORD family (L2) which identified linkage to a 15 cM interval in chromosomal region 11q23.3, flanked by D11S4127 and D11S4151, with a maximum LOD score of 6.77 (Fig. 2). Two clinically indistinguishable L-ORD families (L4–5) were unlinked to this region, consistent with genetic heterogeneity, one of which (L4) also showed a different distribution of sub-RPE deposits compared with linked families (1,2,4).

The flanking markers defined a genomic region spanning 8.7–8.9 Mb containing 90–118 genes ([www.ensembl.org/](http://www.ensembl.org/);

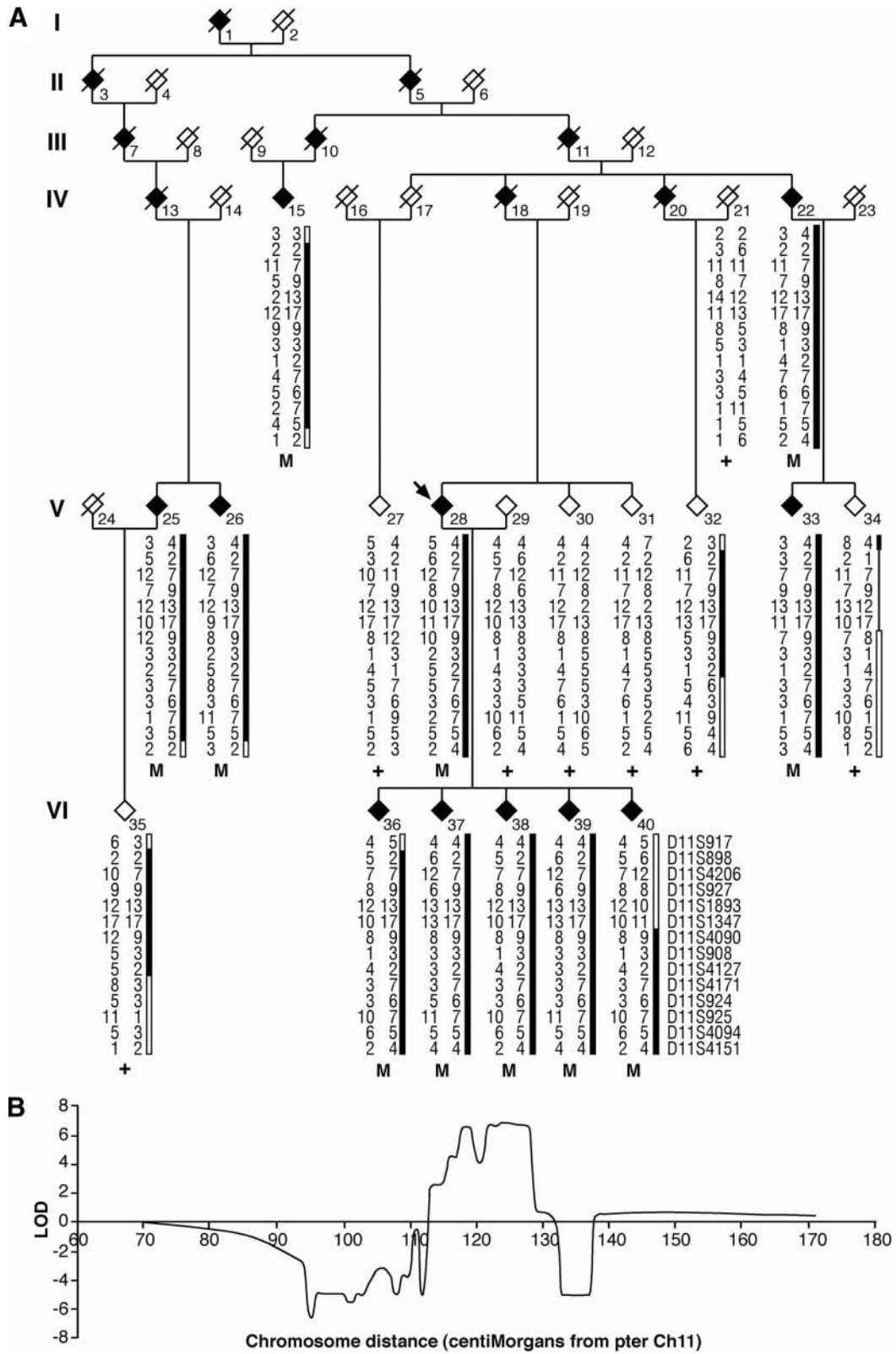


**Figure 2.** Genetic mapping of a L-ORD locus. (A) Haplotypes of L-ORD family L2 are shown with 11q23 markers, in which the disease-associated haplotype is shown as a thick black line. Affected members are shown as solid diamonds and unaffecteds as open diamonds (sexes are not shown for reasons of confidentiality). *CTRP5* mutation carriers are shown with an 'M' and non-carriers with a '+' symbol below the haplotype. (B) Multipoint LOD scores are shown spanning the 11q23 region, showing significant linkage to markers in the interval between D11S4127 proximally (crossover in V-32) and D11S4151 distally (crossovers in individuals IV-15, V-25 and V-26).

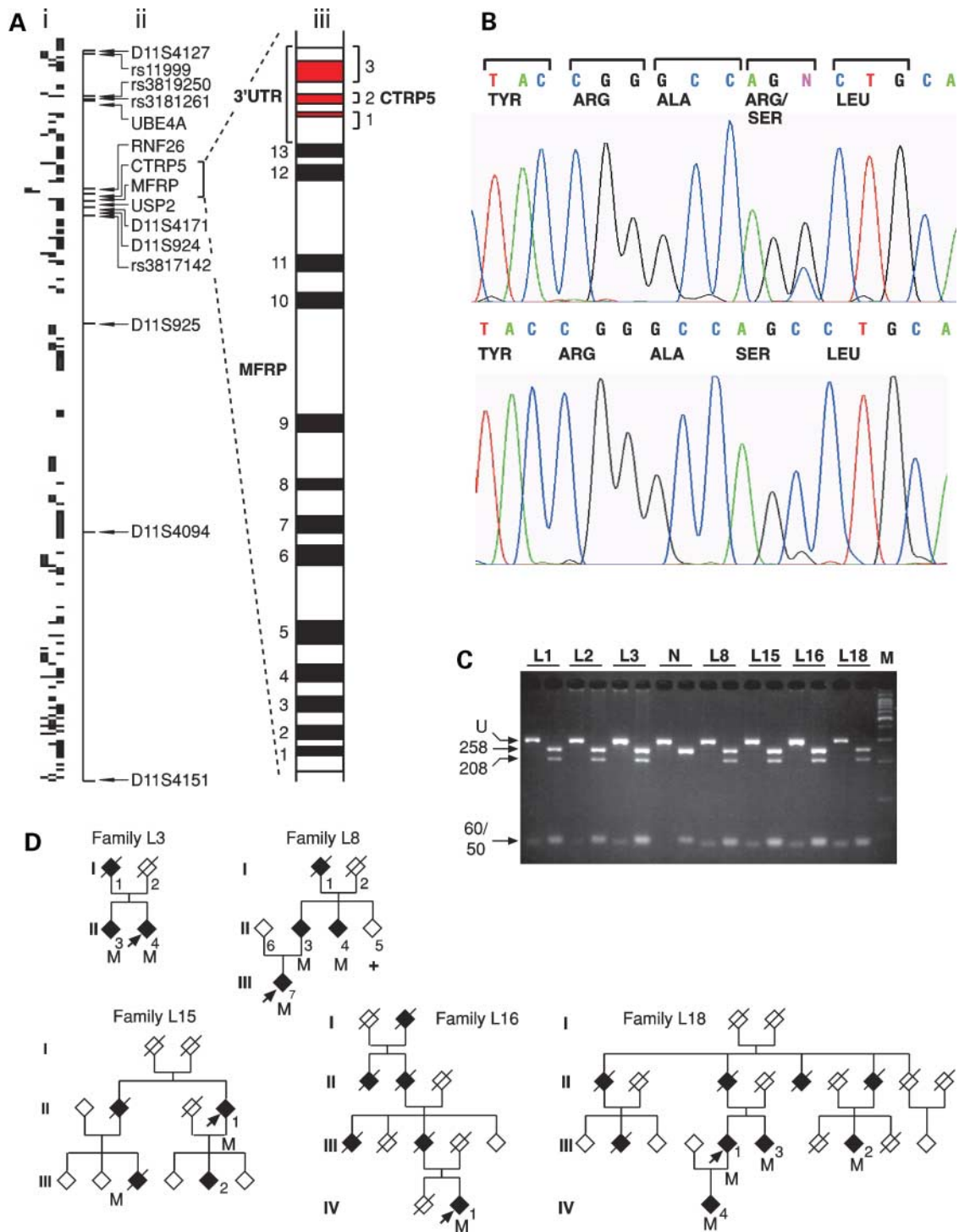


**Figure 3.** Identification of *CTRP5* mutations in L-ORD families. **(A)** Genomic map of the region of search flanked by markers D11S4127 proximally and D11S4151 distally, showing: (i) genes predicted by Ensembl; (ii) markers used in the genetic analysis and excluded candidate genes—*UBE4A*, *RNF26*, *MFRP*, *USP2* (*MMP3*, *BACE*, *PCSK7*, *ORP150* and *ERGB* were also excluded prior to narrowing the disease interval to this extent); and (iii) schematic diagram of the genomic region containing *CTRP5* and its relationship to *MFRP* (12). *CTRP5* is entirely contained within the 3'-untranslated region of the final exon of *MFRP* (exon 13). The 13 exons of *MFRP* (coding regions) are shown as solid rectangles and numbered accordingly on the left of the figure, together with the 3'-untranslated region (3'-UTR). On the right of the figure the three *CTRP5* exons (coding regions) are shown in red (marked 1–3). **(B)** Sequence analysis of *CTRP5* exon 3 showing a heterozygous C to G transversion at codon 163, resulting in a predicted serine to arginine mutation in an affected individual with L-ORD (upper trace) compared with a normal control (lower trace). **(C)** Mutation detection in affected members of seven different L-ORD families using *Bst*NI digests, which generate bands of 258 and 60 bp in normal (Ser163) controls (N), and bands of 208, 60 and 50 bp in mutant (Arg163) carriers. Each family shows the undigested (U) DNA fragment (left track) and digested fragment (right track) with their sizes indicated by arrows. Each affected individual is heterozygous for normal and mutant alleles. M, 100 bp ladder marker. **(D)** L-ORD families L3, 8, 15, 16 and 18 in which the Ser163Arg mutation (M) is found in all affected individuals tested (solid diamonds). Non-carriers of known clinical status are shown with an unfilled diamond above a '+' symbol. Other individuals shown were unavailable for testing.



**Table 1.** Haplotype sharing between the seven L-ORD families with markers flanking the Ser163Arg (S163R) mutation in *CTRP5*, consistent with a founder mutation. The D markers are microsatellites and rs markers are single nucleotide polymorphisms. The distance between markers D11S4127 and D11S925 is 3.18 Mb (<http://genome.ucsc.edu/>). The bold entries indicate the common haplotype

	Family 1	Family 2	Family 3	Family 8	Family 15	Family 16	Family 18
D11S4090	9	9	13	8	9	12	11
D11S908	2	3	3	3	5	2	6
D11S4127	2	2	2	2	2	2	4
rs11999	<b>A</b>	<b>A</b>	<b>A</b>	<b>A</b>	<b>A</b>	<b>A</b>	<b>A</b>
rs3819250	<b>G</b>	<b>G</b>	<b>G</b>	<b>G</b>	<b>G</b>	<b>G</b>	<b>G</b>
rs3181261	<b>G</b>	<b>G</b>	<b>G</b>	<b>G</b>	<b>G</b>	<b>G</b>	<b>G</b>
S163R	<b>163R</b>	<b>163R</b>	<b>163R</b>	<b>163R</b>	<b>163R</b>	<b>163R</b>	<b>163R</b>
D11S4171	7	7	7	7	7	7	7
D11S924	<b>6</b>	<b>6</b>	<b>6</b>	<b>6</b>	<b>6</b>	<b>6</b>	<b>6</b>
rs3817142	<b>G</b>	<b>G</b>	<b>G</b>	<b>G</b>	<b>G</b>	<b>G</b>	<b>G</b>
D11S925	1	7	18	1	10	10	1
D11S4094	4	5	6	5	5	5	5
D11S4151	2	4	8	2	8	8	2

<http://genome.ucsc.edu/>; Fig. 3A). Candidate genes were prioritised and 10 genes excluded before we found a heterozygous C→G transversion at nucleotide 686 in exon 3 of the *CTRP5* gene, resulting in a Ser163Arg substitution (Fig. 3B). This creates a new *Bst*NI restriction site (Fig. 3C), which was absent from 1000 ethnically matched control individuals. The *CTRP5* gene is entirely contained within the last exon of the *MFRP* gene and in the same orientation (Fig. 3A). In mouse and humans (data not shown) both genes are expressed as a bicistronic transcript. This was tested by PCR amplification of retinal cDNA between *MFRP* exon 12 and *CTRP5* exon 3, which gave a product of 1.858 kb, as predicted when both genes are co-expressed. In addition, since the *Mfrp* gene is mutated in the *rd6* mouse retinal degeneration (12), the entire human *MFRP* gene, including all 13 exons and introns, was sequenced, but no mutations were identified.

Alignment of *CTRP5* with its orthologues in seven other species showed that Ser163 is completely conserved in mammals, birds and fish (Fig. 4A). The same Ser163Arg substitution was then found in affected members of seven out of 14 unrelated L-ORD families (Fig. 3C). The presumed Arg163 mutation was found in 28 affected and no unaffected individuals from the seven families (Figs 2A and 3D). However, in one North American family (L1), two apparently affected individuals in one sibship did not carry the mutation, despite the fact that it segregated with disease in other branches of the family. Both individuals (aged 41 and 48 years) had no ocular abnormalities on clinical examination (specifically, no drusen to suggest a phenocopy, such as an early form of AMD), but did have delayed recovery kinetics of dark adaptation, which we have previously shown to be a phenotypic marker for L-ORD (3). This family (L1) originated from within 10 miles of family L2 at the time of their emigration from Scotland in the early 1800s. Haplotype analysis showed that neither of these affected individuals shared an extended 11q23 haplotype with other affected members (see Fig. 1 in Supplementary Material), strongly suggesting that their disease results from some other cause rather than from linkage disequilibrium with a nearby and causal mutation. Based on the existence of other L-ORD families unlinked to the 11q23 region but showing this same phenotype, the disease in these individuals is most likely to result from another molecular cause of L-ORD, which is

reinforced by the uncertainty regarding its prevalence, although subclinical AMD cannot be ruled out. Other examples in which two distinct genes segregate within a single disease kindred have been reported (13,14), due to ascertainment bias in selection of multiple affected families. This explanation was reinforced by showing that a seven-locus haplotype containing the Ser163Arg mutation was common to all seven families, including family L1, defined by markers rs11999–rs3819250–rs3181261–*CTRP5*–D11S4171–D11S924–rs3817142 (alleles A–G–G–163Arg–7–6–G), spanning a distance of 3.18 Mb (Table 1). This suggests that Ser163Arg is a disease-causing founder mutation, since all seven families originated from south-east Scotland, similar to the situation with founder *TIMP3* and *EFEMP1* mutations in other macular degenerations (15,16).

*CTRP5* was initially identified in a cDNA library enriched for genes showing RPE-specific expression (17). Expressed sequence tags (ESTs) have been reported in RPE, retinal fovea, macular and eye libraries and at low levels in several other tissues ([www.ncbi.nlm.nih.gov/](http://www.ncbi.nlm.nih.gov/)). We examined its expression by reverse transcriptase PCR of RNA isolated from eight human tissues and found that it is expressed in RPE, liver, lung, brain and placenta (Fig. 4B).

*CTRP5* is predicted to be a 25 kDa protein with three domains: a signal peptide (residues 1–15), a collagen domain (residues 30–98) containing 23 uninterrupted Gly-X-Y repeats, and a gC1q domain (residues 99–243; Fig. 4A). It is a member of the C1q/tumor necrosis factor superfamily, which shows diverse functions (18–20), including cell adhesion and basement membrane components. The Ser163 residue occurs within the gC1q domain, which in short-chain collagens nucleates trimerization and folding of the collagen stalk and mediates other interactions (18–22).

The normal and mutant gC1q domains were expressed in bacteria as fusion proteins to examine their structure and function. Protein and gel extracts were examined by MALDI-ToF mass spectrometry, which confirmed the identity of mutant and normal fusions and showed that the Arg163 mutant has a stronger tendency to form higher order multimers than the Ser163 fusion. The Arg163 fusion also readily became insoluble *in vitro*, suggesting that it is prone to aggregation, compared with Ser163 (Fig. 5A). In denaturing polyacrylamide gel electrophoresis (PAGE) gels, the Ser163 and Arg163

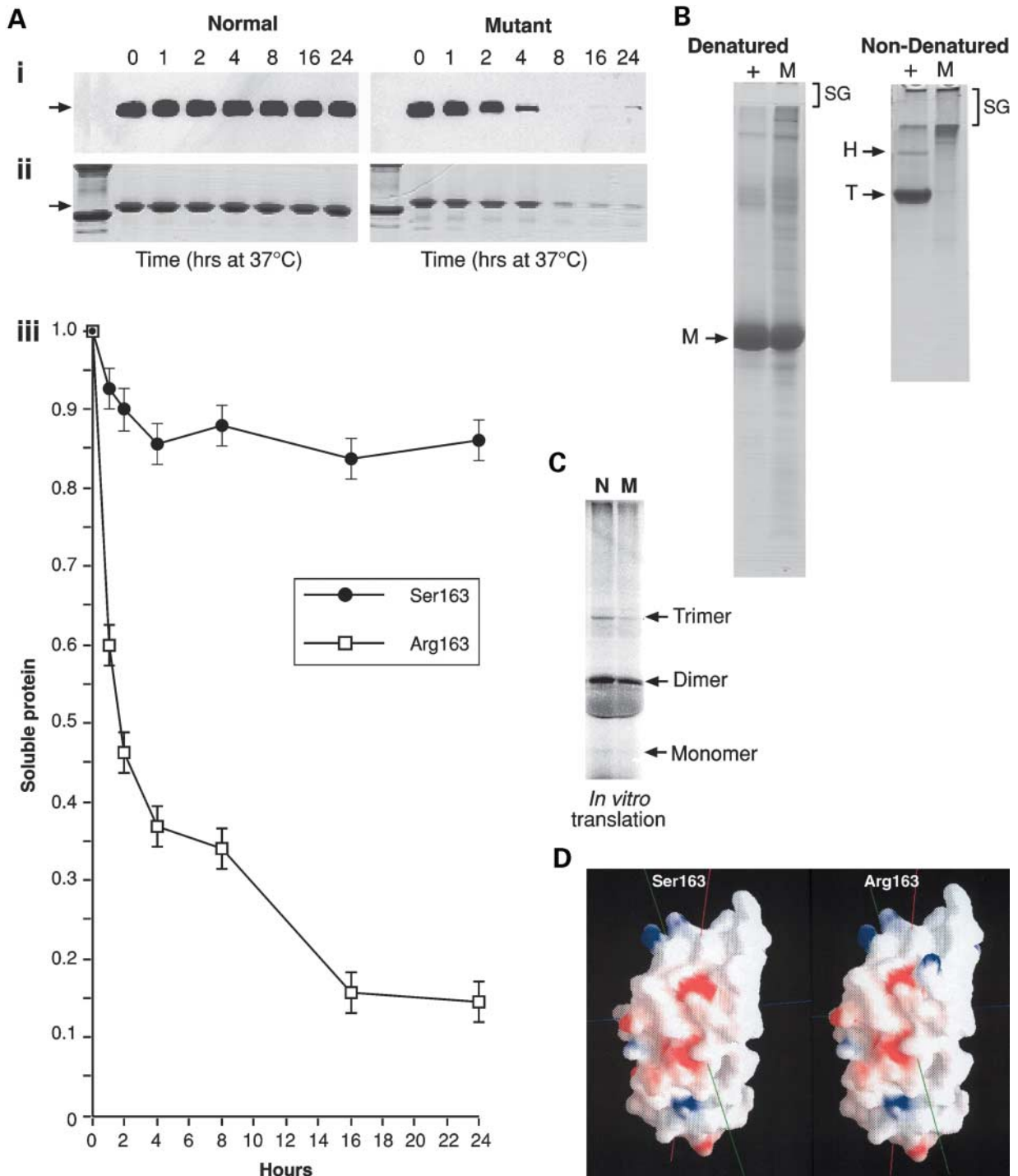


**Figure 5.** Functional analysis of CTRP5 protein. (A) Time course showing changes in solubility at 37°C of thioredoxin-CTRP5 gC1q fusion protein (gC1q fusion) containing normal (Ser) or mutant (Arg) sequence at residue 163. (i) Western blot analysis of a denaturing PAGE gel labelled with anti-His tag antibody and (ii) the corresponding Coomassie stained gel. Arrows indicate the gC1q fusion monomer. The protein concentration remaining in solution at each time point is shown below. The results of three experiments (mean ± SD) show a statistically highly significant difference ( $P < 0.001$ ) between mutant and normal at all times. (B) Comparison of normal (+) and mutant (M) gC1q fusion proteins run on denaturing and non-denaturing PAGE gels. Both show equal amounts of the monomeric (M) form under denaturing conditions. Under non-denaturing conditions, the mutant failed to enter the gel, while the normal protein migrated predominantly as a trimer (T; estimated 97 kDa) with a lesser amount of hexamer (H; estimated 201 kDa). SG, stacking gel. (C) *In vitro* translation of normal (N) and mutant (M) CTRP5 gC1q domain showing that both are able to form monomers, dimers and trimers. (D) Structural model of CTRP5 gC1q domain containing either Ser163 (normal) or Arg163 (mutant). The electrostatic surface was drawn by the program GRASP (32) for the models described in Methods. The red regions indicate negatively charged regions corresponding to the carboxylate groups of the protein, and the blue regions positively charged regions from Arg, Lys and N-terminal amino groups. The effect of the mutation can be clearly seen. The  $x$ ,  $y$  and  $z$  axes of the co-ordinate frame used by the program are shown as blue, green and red, respectively.

fusions both showed a major monomeric species (Fig. 5B). In contrast, the Arg163 mutant was unable to enter non-denaturing PAGE gels, while Ser163 migrated as a major trimeric and weak hexameric species (Fig. 5B). The Arg163 mutant therefore forms high molecular weight aggregates that are not detected with the normal protein. Finally, fresh *in vitro* translated gC1q domains containing Ser163 or Arg163 were both able to form trimers (Fig. 5C), suggesting that this residue is not directly involved in trimerisation (see below).

Comparative protein modelling of Ser163 and Arg163 gC1q domains were analysed using a model (23), based on the crystal structures of adiponectin (20) and collagen X (21), which showed good correspondence with both templates. The Ser163Arg mutation occurs in a surface loop and produces a significant positive patch on the protein surface, remote from the trimer interface (Fig. 5D). It is tempting to speculate that the observed aggregation results from heterologous association of this positive patch with a negative patch elsewhere on the molecular surface.

## DISCUSSION

Few genes are capable of individually reproducing major pathological features of common multifactorial diseases (24). Those that do generally involve primary and rate-determining steps in the disease process and provide important mechanistic insights. In AMD, macular drusen and neovascularization are important focal features but these either appear late in the disease process (choroidal neovascularization) or, in the case of drusen, are not a prominent disease feature in some ethnic groups. This suggests that the most compelling primary aetiological factor in AMD is the presence of diffuse macular extracellular deposits between RPE and Bruch's membrane, which thicken and become lipid-laden with age (6,25). In L-ORD, the deposit shows earlier onset and is more extensive than in AMD but is otherwise hard to distinguish (1–5). Among proposed 'genetic models' of AMD, only SFD, which results from mutations in *TIMP3*, shares this important pathological feature (9).

The fact that the major clinical features of AMD are each found in L-ORD, at various stages of the disease, suggests that the normal L-ORD gene has an important and primary role in prevention of both diseases. These common features include: (i) diffuse sub-RPE deposits that are indistinguishable at the light microscope level from those seen in AMD, although these extend into the peripheral retina in L-ORD (1,2,4,5); (ii) macular degeneration associated with abnormal dark adaptation kinetics (1–3,10,11); (iii) drusen-like sub-RPE deposits in the early to middle stages of the disease (1–3); and (iv) choroidal neovascularisation and disciform scarring (1,2,4,5). Although the question as to whether mutations in *CTRP5* influence susceptibility to AMD remains to be resolved, the identification of a *CTRP5* mutation that can reproduce so many features of AMD shows that this finding alone provides a new insight into fundamental disease mechanisms in both diseases. *CTRP5* has been proposed to interact with the CUB domain of *MFRP* and preliminary yeast two-hybrid results are consistent with this (data not shown), suggesting that a novel Wnt/Frizzled pathway is implicated in both L-ORD and AMD, as it is in the *rd6* mouse.

AMD is one of the commonest diseases in the elderly and is likely to be both multifactorial and highly polygenic in nature (7,24). Understanding of pathogenetic mechanisms in such common diseases has been accordingly hard to obtain but progress has been greatest where genes responsible for comparatively rare Mendelian models of such disorders have been identified. Few of these genes individually have any impact on the common disease *per se* and yet they have highlighted primary disease pathways in coronary artery disease, breast and colon cancer, type 2 diabetes mellitus, Alzheimer disease and numerous others (24).

Disease-causing mutations occur in short-chain collagens VIII and X, including its gC1q domain (26,27). The presence of a non-conservative missense mutation in the gC1q domain of *CTRP5* in a highly conserved residue in 7/14 L-ORD families and 0/1000 control individuals suggests that it is a disease-causing founder mutation, similar to those seen in Doyme honeycomb retinal dystrophy (*EFEMP1*) and SFD (*TIMP3*) (15,16). The only discrepancy is the presence of two apparently affected siblings in one family (L1) who neither carry the mutation nor share the linked 11q23 chromosomal region, suggesting that their disease results from another cause. The most plausible explanation is that, since L-ORD is genetically heterogeneous, the disease in these individuals results from segregation at another locus within this branch of the family, as a result of ascertainment bias arising from identification of multiple affected member families. This has been reported in at least two other families, a rare early-onset autosomal dominant glaucoma family and a large consanguineous retinitis pigmentosa kindred (13,14). However, the Ser163Arg mutation in *CTRP5* was present in 28 affected members of seven apparently unrelated L-ORD kindreds and no normal controls, and shows both abnormal stability and a tendency to aggregation *in vitro*, strongly suggesting that it is the disease-causing mutation in these families. At least two of the remaining seven L-ORD families appear to be unlinked to the 11q23 region, so that these almost certainly result from mutation in one or more additional L-ORD genes.

The close relationship of *CTRP5* to *MFRP* raises the issue of whether the causal mutation in L-ORD could lie within *MFRP*, which is already known to cause retinal degeneration in the *rd6* mouse (12). This possibility has firstly been excluded by sequence analysis of the entire *MFRP* gene in all seven L-ORD families carrying the Ser163Arg mutation in *CTRP5*. However, the possibility of a regulatory or cryptic mutation in *MFRP* cannot be completely excluded. However, two other arguments make the possibility of a primary *CTRP5* mutation more compelling. Firstly, most genes expressed as dicistronic transcripts are functionally related (12) so that the possibility that either or both genes can cause similar disease is reasonable. Preliminary data from yeast two-hybrid experiments show that *CTRP5* and *MFRP* do indeed interact directly (data not shown). Secondly, both functional and structural analyses of the mutant *CTRP5* protein strongly indicate that it is potentially pathogenic, due to its instability and tendency to aggregation, the non-conservative nature of the substitution and conserved site of the mutation. Finally, the alternative possibility that the *rd6* *Mfrp* mutation in fact results from mutation or functional impairment of *C1qtnf5* (*Ctrp5*), or of both genes, is again unlikely. Firstly, *C1qtnf5* was excluded by sequence analysis

(12). Secondly, the *rd6* mutation is a 4 bp deletion immediately adjacent to the conserved exon 4 splice site, which causes in-frame deletion of exon 4, encoding 58 amino acids lying between the transmembrane segment and first CUB domain within the presumptive extracellular region. The consequences of this deletion on MFRP function remain to be shown but it is unlikely to interfere with transcription of *C1qtnf5* as a result of mechanisms such as nonsense-mediated decay.

CTRP5 appears to be secreted by RPE and preliminary data (not shown) suggest that it is a constituent of Bruch's membrane. By analogy with collagens VIII and X, and probably saccular collagen (18,19,26,27), it may form an extracellular hexagonal lattice, facilitating the adhesion of basal RPE to Bruch's membrane. The Ser163Arg mutation is likely to impair this adhesion, leading to the build-up of extracellular deposits. This contrasts with the situation in SFD, in which it is proposed that mutant TIMP3 accumulates in Bruch's membrane, and is associated with abnormal metalloproteinase and/or vascular endothelial growth factor activity within the membrane (28,29).

CTRP5 is similar to adiponectin, C1q peptides and short-chain collagens VIII and X, which share a similar genomic structure, suggesting a common origin (18,19). It consists of a short amino-terminal collagenous domain followed by a globular C1q domain, which is proposed to be necessary for 'zippering' and trimerization of the collagen domain (18,19). The instability of the Arg163 mutant gC1q domain *in vitro* suggests that it may be associated either with loss-of-function due to haploinsufficiency or gain-of-function due to protein aggregation. In each case, the result may be impaired adhesion between RPE and Bruch's membrane, leading to build up of extracellular material shed by RPE or diffusing from choroidal vessels to RPE. The precise role of CTRP5 remains to be established but the presence of a common founder mutation in L-ORD suggests that this protein exerts an important influence on the build-up of extracellular deposits with age, as seen in both L-ORD and AMD.

## MATERIALS AND METHODS

### Patient ascertainment and diagnoses

Research procedures were in accordance with institutional guidelines and the tenets of the Declaration of Helsinki. Fourteen families with L-ORD were ascertained from genetic eye clinics in Edinburgh and Philadelphia. Eleven families either included autopsy evidence of L-ORD (L1, L3–4) or evidence of L-ORD based on clinical and psychophysical criteria (1–3) plus autosomal dominant inheritance ('definite' L-ORD; L2, L5–8, L12–14). Three L-ORD families (L15–16, L18) were diagnosed on the basis of clinical criteria and autosomal dominant inheritance ('probable' L-ORD). Unaffected individuals were assumed to be normal only if they were clinically examined (by S.G.J.) and showed normal two-colour dark adaptometry after age 50 years, whereas those under age 50 years were assumed to be of status unknown. Retinal regional variation of the dark-adaptation abnormality was quantified by comparing the results within the macula to more peripheral retina. Dark-adaptation functions were

obtained at 16 loci from 4 to 40° (1.3–13 mm) eccentric along the horizontal meridian, and from 4 to 20° in the vertical meridian; bright full field white flashes (6.2 log scot-tds; ~14% bleach) were used as the adapting light. The extent of dark-adaptation abnormality was quantified by determining the time to reach 3.5 log sensitivity adjusted by the mean normal value.

### Histopathology and immunohistochemistry

Post-mortem human eyes were obtained through the Foundation Fighting Blindness and University of Washington Lions Eye Bank. A retina with L-ORD (80-year-old woman, 6.25 h post mortem; family L1) and a normal retina (60-year-old man, 3.25 h post-mortem) were fixed, stored and processed by published methods (1,2). Clinical details about this L-ORD patient-donor (at age 75) were previously reported (patient III-4) (1). Sections (4 µm) were stained with Richardson's methylene blue/azure II.

### Genetic mapping

A 400 marker genome scan was carried out using the ABI HD10 set of micro satellite markers, spaced at 10 cM intervals, and run on an ABI3700 automated genotyper. Genotypes were analysed and checked using ABI Genescan and Genotyper software. Allele frequencies were obtained from the CEPH database and genetic distances from Kong *et al.* (30). The disease gene frequency was set at 0.0001. The disease haplotype was established by comparing the results of 10 markers (six microsatellites and four single-nucleotide polymorphisms (SNPs) flanking *CTRP5* (cen–D11S4127–rs11999–rs3819250–rs3181261–*CTRP5*–D11S4171–D11S924–rs3817142–D11S925–D11S4094–D11S4151–qter). SNPs were analysed by direct sequencing. Linkage analyses were performed using the LINKAGE programme package (31) with serial multipoint LODS calculated from LINKMAP data by interpolation. Individuals tested 'normal' after age 50 were taken to be unaffected; those under this age were assigned status unknown.

### Candidate gene analyses

Candidate genes were analysed by direct sequencing using the ABI Big-DYE version 2 sequencing kit. *CTRP5* primer sequences used for mutation analysis are shown in Table 1 of Supplementary Material. The Ser163Arg mutation was confirmed by sequencing of both strands following PCR using the forward primer 5'-ACG AGC AGG GAC ATT ACG AC and reverse primer 5'-AGA AAT CCG GAG AAG GTG CT. The same PCR fragment was used for further confirmation of the mutation and screening by restriction digestion with *Bst*NI (New England Biolabs) according to the manufacturer's protocol, which gave bands of 258 and 60 bp (normal, Ser163) or 208, 50 and 60 bp (mutant, Arg163).

### Expression analysis

Total RNA was isolated using TRIZOL (Invitrogen). First-strand cDNA was generated from 2.5 µg of total RNA by priming with oligo-dT followed by reverse transcription

(www.invitrogen.com). Primers for *CTRP5* were designed to span a 490 bp region based on cDNA sequence. Forward primer is located at position 248 within exon 2 (5'-CCCACTGGACGACAACAAG). Reverse primer is located at position 737 within exon 3 (5'-CTGGAAGAAAGAGG CAATGG). Since the primers span an intron, products from genomic contamination could be distinguished from products resulting from cDNA. Primers for HPRT yielded a 386 bp product from cDNAs (F, 5'-ACCCCACGAAGTGTGGATA; R; 5'-TAAACAACAATCCGCCCAAA). These primers span ~1.5 kb of intronic sequence, thus products are based on cDNA and not genomic DNA contamination. PCR reactions were performed using standard conditions.

### Functional analysis of CTRP5

*CTRP5* expression and purification. The gC1q domain of human CTRP5 (residues 100–243) was PCR amplified from normal (163Ser) or mutant (163Arg) genomic DNA using forward primer 5'-GGA TCC GTG CCT CCG CGA TCC GCC TTC and reverse primer 5'-AGC AAA GAC TGG GGA GCT GTG GGA GCT using standard PCR conditions. Products were ligated into an N-terminal thioredoxin fusion vector, pBAD/Thio-TOPO (Invitrogen), containing a C-terminal hexa-Histidine epitope tag and transformed into *E. coli* strain LMG194. Expression was induced with 0.02% arabinose at 18°C, and the cells centrifuged and disrupted using a French press in cell lysis buffer (150 mM NaCl, 50 mM Tris-HCl, 10% glycerol, pH 8.0) containing proteinase inhibitors (Roche). The cell lysate was centrifuged for 30 min at 13 000 rpm, and fusion protein was purified with Ni-NTA superflow (QIAGEN), following the manufacturer's instructions. The proteins were added to 2× loading buffer (1% SDS, 20 mM Tris-HCl pH 6.8, 20% sucrose) and analysed by SDS-PAGE, after which the gel was stained with Coomassie Blue R250 or transferred to nitrocellulose membrane for western analysis, using anti-His Tag antibody (1:5000; Clontech) and HRP-labelled anti-mouse antibody (1:5000). Native (non-denaturing) gels were prepared by omitting SDS and dithiothreitol from the standard Laemmli SDS-PAGE protocol and bands were sized using non-denatured molecular weight standards (Sigma) run on 6, 8, 10 and 12% gels, following the manufacturer's protocol.

Co-transcription of *MFRP* and *CTRP5* was tested by PCR amplification of retinal cDNA (Clontech) using the forward primer 5'-ACA CCA CAG CCT TCC CTA ACA TCT (*MFRP* exon 12) and reverse primer 5'-GCT GGC ATA GAT GCC AAT GTA GTC (*CTRP5* exon 3), which gave a product of 1.858 kb, as predicted when both genes are co-expressed. PCR was carried out using the Expand High Fidelity PCR System (Roche) and standard conditions.

*Protein solubility.* Aliquots of purified protein (normal or mutant) were kept at 37°C for 1, 2, 4, 8, 16 or 24 h, then centrifuged at 12 000 rpm for 10 min, and 10 µl aliquots analysed by SDS-PAGE and western blot. The concentrations of 20 µl aliquots were determined from the absorbance at 595 nm using the Coomassie Plus protein assay reagent, according to the manufacturer's instructions (Pierce). The time course data were evaluated by analysis of variance using the ratio of all protein

concentrations compared with time zero. Tests for homogeneity of variance were satisfied and standard errors were pooled over all groups.

*In vitro translation.* Normal and mutant CTRP5 gC1q domains (positions 97–243) were cloned after PCR amplification from normal and patient genomic DNA using forward primer 5'-ATG GAG TGC TCG GTG CCT CCG CGA and reverse primer 5'-AGC AAA GAC TGG GGA GCT GTG, and standard PCR conditions. The products were ligated into pCR-TOPO 2.1 (Invitrogen) and checked by sequencing. *In vitro* expression was carried out using the TNT T7 Quick couple transcription/translation system (Promega), in which 1 µg of purified construct was expressed in 40 µl of TNT Quick Master Mix containing 2 µl [<sup>35</sup>S]-methionine (>1000 Ci/mmol, Amersham) made up to a final volume of 50 µl with sterile distilled water. The reaction was incubated at 30°C for 90 min. Aliquots of 5 µl of each reaction were added to 40 µl sample buffer (10 mM Tris-HCl, pH 6.8, 0.5% SDS, 20% sucrose). All samples were resolved on standard 12% PAGE gels containing 0.1% SDS. Gels were fixed, dried and exposed to Kodak Biomax Film.

*Mass spectrometry analysis.* Matrix-assisted laser desorption ionisation time of flight (MALDI-ToF) analysis was performed on peptides extracted from PAGE gels after trypsin digestion or on whole protein extracts using a Voyager-DE STR Biospectrometry Workstation (Applied Biosystems). A mass spectrum was obtained which confirmed that each of the excised bands were thioredoxin-gC1q fusion protein; over 70% sequence coverage was achieved for both normal and mutant peptides. A mass at 1089.642 Da was only observed in the mutant and this was assigned to residues 162–170 (ARLQFDLVK), containing the 163Arg mutation. A Q-ToF I (Micromass UK) was used to sequence residues 115–127 and 110–114 from both the Ser163 and Arg163 forms.

*Protein alignments.* Public databases (dbEST, GenBank and others) were searched using the tblastn software available at NCBI (www.ncbi.nlm.nih.gov/) to identify CTRP5 orthologues in other species (mouse, rat, bovine, chicken, *Fugu rubripes*, zebrafish and rainbow trout). The alignment with human CTRP5 was carried using the Clustalw tool, available at the European Bioinformatics Institute (www.ebi.ac.uk/).

*Molecular modelling.* The amino acid sequences for the normal CTRP5 gC1q domain and Ser163Arg mutant were pasted separately into the SWISS-MODEL software package (23) (<http://swissmodel.expasy.org/>), using the First Approach mode with the supplied defaults. With the mutant sequence, two models were found, firstly, the A-chain of type X collagen [1gr3;  $P(N) = 4 \times 10^{-21}$ ; 41% identity] and secondly, all three chains of adiponectin [1c28;  $P(N) = 4 \times 10^{-20}$ ,  $9 \times 10^{-18}$ ,  $2 \times 10^{-14}$ ; 45, 38, 53% identity]. Similar results were obtained with the normal sequence. Models were produced automatically for the C-terminal portion

of the protein between residues Glu112 and Ser239, and used without further refinement to generate an electrostatic surface, using the defaults in the program GRASP (32).

## SUPPLEMENTARY MATERIAL

Supplementary Material is available at HMG Online.

## ACKNOWLEDGEMENTS

We thank the Foundation Fighting Blindness, British Retinitis Pigmentosa Society, Macula Vision Research Foundation, Macular Disease Foundation, Medical Research Council and National Institutes of Health (EY13385, 13729, 13203) for financial support. We also thank Dr P. Bishop, Dr K. Sawin, Dr T. Aleman and L. Mack for help and advice; P. Teague for help with statistical analyses; J. Emmons, D. Hanna and S. Schwartz for clinical coordinating; Dr A.-M. Armbrrecht and Dr E. Wright for clinical sampling; and D. Stuart for the artwork.

## REFERENCES

- Kuntz, C.A., Jacobson, S.G., Cideciyan, A.V., Li, Z.Y., Stone, E.M., Possin, D. and Milam, A.H. (1996) Sub-retinal pigment epithelial deposits in a dominant late-onset retinal degeneration. *Invest. Ophthalmol. Visual Sci.*, **37**, 1772–1782.
- Milam, A.H., Curcio, C.A., Cideciyan, A.V., Saxena, S., John, S.K., Kruth, H.S., Malek, G., Heckenlively, J.R., Weleber, R.G. and Jacobson, S.G. (2000) Dominant late-onset retinal degeneration with regional variation of sub-retinal pigment epithelium deposits, retinal function, and photoreceptor degeneration. *Ophthalmology*, **107**, 2256–2266.
- Jacobson, S.G., Cideciyan, A.V., Wright, E. and Wright, A.F. (2001) Phenotypic marker for early disease detection in dominant late-onset retinal degeneration. *Invest. Ophthalmol. Visual Sci.*, **42**, 1882–1890.
- Duvall, J., McKechnie, N.M., Lee, W.R., Rothery, S. and Marshall, J. (1986) Extensive subretinal pigment epithelial deposit in two brothers suffering from dominant retinitis pigmentosa. A histopathological study. *Graefes Arch. Clin. Exp. Ophthalmol.*, **24**, 299–309.
- Brosnahan, D.M., Kennedy, S.M., Converse, C.A., Lee, W.R. and Hammer, H.M. (1994) Pathology of hereditary retinal degeneration associated with hypobetalipoproteinemia. *Ophthalmology*, **101**, 38–45.
- Green, W.R. and Enger, C. (1993) Age-related macular degeneration histopathologic studies: the 1992 Lorenz E. Zimmerman Lecture. *Ophthalmology*, **100**, 1519–1535.
- Seddon, J.M. (2001) Age-related macular degeneration. In Ryan, S.J. (ed.), *Retina* (3rd edn), Mosby, St Louis, MO, pp. 1039–1050.
- Crabb, J.W., Miyagi, M., Gu, X., Shadrach, K., West, K.A., Sakaguchi, H., Kamei, M., Hasan, A., Yan, L., Rayborn, M.E. et al. (2002) Drusen proteome analysis: an approach to the etiology of age-related macular degeneration. *Proc. Natl Acad. Sci. USA*, **99**, 14682–14687.
- Weber, B.H., Vogt, G., Pruett, R.C., Stohr, H. and Felbor, U. (1994) Mutations in the tissue inhibitor of metalloproteinases-3 (TIMP3) in patients with Sorsby's fundus dystrophy. *Nat. Genet.*, **8**, 352–356.
- Owsley, C., Jackson, G.R., White, M., Feist, R. and Edwards, D. (2001) Delays in rod-mediated dark adaptation in early age-related maculopathy. *Ophthalmology*, **108**, 1196–1202.
- Haimovici, R., Owens, S.L., Fitzke, F.W. and Bird, A.C. (2002) Dark adaptation in age-related macular degeneration: relationship to the fellow eye. *Graefes Arch. Clin. Exp. Ophthalmol.*, **40**, 90–95.
- Kameya, S., Hawes, N.L., Chang, B., Heckenlively, J.R., Naggert, J.K. and Nishina, P.M. (2002) *Mfrp*, a gene encoding a frizzled related protein, is mutated in the mouse retinal degeneration 6. *Hum. Mol. Genet.*, **11**, 1879–1886.
- van Soest, S., Ingeborgh van den Born, L., Gal, A., Farrar, G.J., Bleeker-Wagemakers, L.M., Westerveld, A., Humphries, P., Sandkuijl, L.A. and Bergen, A.A. (1994) Assignment of a gene for autosomal recessive retinitis pigmentosa (RP12) to chromosome 1q31–q32.1 in an inbred and genetically heterogeneous disease population. *Genomics*, **22**, 499–504.
- Angius, A., Spinelli, P., Ghilotti, G., Casu, G., Sole, G., Loi, A., Totaro, A., Zelante, L., Gasparini, P. et al. (2000) Myocilin Gln368stop mutation and advanced age as risk factors for late-onset primary open-angle glaucoma. *Arch. Ophthalmol.*, **118**, 674–679.
- Stone, E.M., Lotery, A.J., Munier, F.L., Heon, E., Piguat, B., Guymer, R.H., Vandenberg, K., Cousin, P., Nishimura, D., Swiderski, R.E. et al. (1999) A single EFEMP1 mutation associated with both Malattia Leventinese and Doyme honeycomb retinal dystrophy. *Nat. Genet.*, **22**, 199–202.
- Wijesuriya, S.D., Evans, K., Jay, M.R., Davison, C., Weber, B.H., Bird, A.C., Bhattacharya, S.S. and Gregory, C.Y. (1996) Sorsby's fundus dystrophy in the British Isles: demonstration of a striking founder effect by microsatellite-generated haplotypes. *Genome Res.*, **6**, 92–101.
- Agarwal, N., Swaroop, A., Zheng, K., Liou, J.D., O'Rourke, K., Graves, K.A., Gieser, L., Del Monte, M. and Yang-Feng, T.L. (1995) Expression and chromosomal localization of cDNA clones from an enriched human retinal pigment epithelial (RPE) cell line library: identification of two RPE-specific genes. *Cytogenet. Cell Genet.*, **69**, 71–74.
- Kishore, U., Kojouharova, M.S. and Reid, K.B. (2002) Recent progress in the understanding of the structure–function relationships of the globular head regions of C1q. *Immunobiology*, **205**, 355–364.
- Kishore, U. and Reid, K.B. (2000) C1q: structure, function, and receptors. *Immunopharmacology*, **49**, 159–170.
- Shapiro, L. and Scherer, P.E. (1998) The crystal structure of a complement-1q family protein suggests an evolutionary link to tumor necrosis factor. *Curr. Biol.*, **8**, 335–338.
- Bogin, O., Kvensakul, M., Rom, E., Singer, J., Yayon, A. and Hohenester, E. (2002) Insight into Schmid metaphyseal chondrodysplasia from the crystal structure of the collagen X NC1 domain trimer. *Structure (Camb.)*, **10**, 165–173.
- Kwan, A.P., Cummings, C.E., Chapman, J.A. and Grant, M.E. (1991) Macromolecular organization of chicken type X collagen *in vitro*. *J. Cell Biol.*, **114**, 597–604.
- Guex, N. and Peitsch, M.C. (1997) SWISS-MODEL and the Swiss-ProtViewer: an environment for comparative protein modelling. *Electrophoresis*, **18**, 2714–2723.
- Wright, A., Charlesworth, B., Rudan, I., Carothers, A. and Campbell, H. (2003) A polygenic basis for late-onset disease. *Trends Genet.*, **19**, 97–106.
- Guymer, R., Luthert, P. and Bird, A. (1999) Changes in Bruch's membrane and related structures with age. *Prog. Retin. Eye Res.*, **18**, 59–90.
- Biswas, S., Munier, F.L., Yardley, J., Hart-Holden, N., Perveen, R., Cousin, P., Sutphin, J.E., Noble, B., Batterbury, M., Kieley, C. et al. (2001) Missense mutations in COL8A2, the gene encoding the alpha2 chain of type VIII collagen, cause two forms of corneal endothelial dystrophy. *Hum. Mol. Genet.*, **10**, 2415–2423.
- Marks, D.S., Gregory, C.A., Wallis, G.A., Brass, A., Kadler, K.E. and Boot-Handford, R.P. (1999) Metaphyseal chondrodysplasia type Schmid mutations are predicted to occur in two distinct three-dimensional clusters within type X collagen NC1 domains that retain the ability to trimerize. *J. Biol. Chem.*, **274**, 3632–3641.
- Arris, C.E., Bevitt, D.J., Mohamed, J., Li, Z., Langton, K.P., Barker, M.D., Clarke, M.P. and McKie, N. (2003) Expression of mutant and wild-type TIMP3 in primary gingival fibroblasts from Sorsby's fundus dystrophy patients. *Biochim. Biophys. Acta*, **1638**, 20–28.
- Qi, J.H., Ebrahim, Q., Moore, N., Murphy, G., Claesson-Welsh, L., Bond, M., Baker, A. and Anand-Apte, B. (2003) A novel function for tissue inhibitor of metalloproteinases-3 (TIMP3): inhibition of angiogenesis by blockage of VEGF binding to VEGF receptor-2. *Nat. Med.*, **9**, 407–415.
- Kong, A., Gudbjartsson, D.F., Sainz, J., Jonsson, G.M., Gudjonsson, S.A., Richardson, B., Sigurdardottir, S., Barnard, J., Hallbeck, B., Masson, G. et al. (2002) A high-resolution recombination map of the human genome. *Nat. Genet.*, **31**, 241–247.
- Lathrop, G.M. and Lalouel, J.M. (1988) Efficient computations in multilocus linkage analysis. *Am. J. Hum. Genet.*, **42**, 498–505.
- Nicholls, A., Bharadwaj, R. and Honig, B. (1993) GRASP: a graphical representation and analysis of surface properties. *Biophys. J.*, **64**, A166.